Light- and Thermal-Induced Spin Crossover in $\{Fe(abpt)_2[N(CN)_2]_2\}$. Synthesis, Structure, Magnetic Properties, and High-Spin ↔ Low-Spin Relaxation Studies

Nicolás Moliner,[1a] Ana B. Gaspar,[1a] M. Carmen Muñoz,[1b] Virginie Niel,[1a] Joan Cano,[1a] and José Antonio Real*,[1a]

Departament de Química Inorgánica/Institut de Ciencia Molecular, Universitat de València, Doctor Moliner 50, E-46100 Burjassot, València, Spain, and Departament de Física Aplicada, Universitat Politécnica de València, Camino de Vera s/n, E-46071, València, Spain

Received January 24, 2001

$\{Fe(abpt)_2[N(CN)_2]_2\}$ (abpt = 4-amino-3,5-bis(pyridin-2-yl)-1,2,4-triazole) represents the first example of an iron(II) spin-crossover compound containing dicyanamide ligand, $[N(CN)_2]^-$, as a counterion. It shows an incomplete two-step spin transition with around 37% of HS molecules trapped in the low-temperature region when standard cooling or warming modes, i.e., 1−2 K min^{-1}, were used. The temperature, $T_{1/2} \approx 86$ K, at which 50% of the conversion takes place, is one of the lowest temperatures observed for an iron(II) spin-crossover compound. Quenching experiments at low temperatures have shown that the incomplete character of the conversion is a consequence of slow kinetics. The quenched HS state relaxes back to the LS state displaying noticeable deviation from a single-exponential law. The rate of relaxation was evaluated in the range of temperatures 10−60 K. In the upper limit of temperatures, where thermal activation predominates, the activation energy and the pre-exponential parameter were estimated as $E_a \approx 280$ cm^{-1} and $A_{HL} \approx 10$ s^{-1}, respectively. The lowest value of k_{HL} around 1.2×10^{-4} s^{-1} ($T = 10$ K) was obtained in the region of temperatures where tunneling predominates. A quantitative light induced excited spin state trapping (LIESST) effect was observed, and the HS → LS relaxation in the range of temperatures 5−52.5 K was studied. From the Arrhenius plot the two above-mentioned characteristic regimes, thermal-activated ($E_a \approx 431$ cm^{-1} and $A_{HL} \approx 144$ s^{-1}) and tunneling ($k_{HL} \approx 1.7 \times 10^{-6}$ s^{-1} at 5 K), were characterized. The crystal structure was solved at room temperature. It crystallizes in the triclinic $P\bar{1}$ space group, and the unit cell contains a centrosymmetric mononuclear unit. Each iron atom is in a distorted octahedral environment with bond distances Fe−N(1) = 2.216(2) Å, Fe−N(2) = 2.121(2) Å, and Fe−N(3) = 2.160(2) Å for the pyridine, triazole, and dicyanamide ligands, respectively.

Introduction

Six-coordinate iron(II) complexes may occur in a high-spin (HS) or low-spin (LS) state depending on whether ligand field strength is weak or strong, respectively. For intermediate ligand fields, the energy gap between the excited state HS and the ground state LS may fall in the range of the thermal energy. Consequently, a crossover (LS ↔ HS) between the two states can be induced by variation of temperature or pressure or by irradiation with light. This fact makes iron(II) spin-crossover compounds a singular class of molecular magnetic materials. They change reversibly from paramagnetic (HS) to diamagnetic (LS) under the effect of the above-mentioned constraints. Optical properties are quite different too for the two spin states; hence a strong color change is observed in the case in which no MLCT absorption bands are present in the d−d region of the electronic spectra.[2]

The LS ↔ HS crossover involves a transfer of two electrons from the e_g to the t_{2g} orbitals. Because of the antibonding nature of the e_g orbitals, a concomitant change of the metal-to-ligand bond distances takes place, being around 0.2 Å shorter in the LS state. Thermal-induced spin crossover is an entropy-driven phenomenon.[3] The entropy term, $T\Delta S$, compensates the energy gap between the two spin states. The different spin multiplicity and density of vibrational states associated with both spin states are the main sources of entropy. In solution molecules are diluted and the thermal evolution of the system follows the Boltzmann law. In contrast, in the solid state intermolecular interactions make the phenomenon cooperative; hence a first-order phase transition with thermal hysteresis may occur.[4]

At low temperatures, usually below 50 K, the rate of the HS ↔ LS process is very small or almost temperature-independent. At these temperatures, the transformation takes place mainly via the quantum tunneling regime. At higher temperatures, both tunneling and thermal activation regimes are responsible for kinetics. However, at temperatures as high as 120 K the transformation may be considered as a thermally activated process that follows the Arrhenius law. For compounds with $T_{1/2} = 100-200$ K the rate constant k_{HL} ranges typically from 10^6 up to 10^{-6} s^{-1}; $T_{1/2} = \Delta H/\Delta S$ is the characteristic temperature of the spin transition.[5]

Most iron(II) spin-crossover complexes have the $[FeN_6]$ core. They can be classified in two main families. One family includes

(1) (a) Departament de Química Inorgánica/Institut de Ciencia Molecular, Universitat de València. (b) Departament de Física Aplicada, Universitat Politécnica de València.

(2) (a) Goodwin, H. A. *Coord. Chem. Rev.* **1976**, *18*, 293. (b) Gütlich, P. *Struct. Bonding (Berlin)* **1981**, *44*, 83. (c) Gütlich, P.; Hauser, A.; Spiering, H. *Angew. Chem., Int. Ed. Engl.* **1994**, *33*, 2024. (d) König, E.; Ritter, G.; Kulshreshtha, S. K. *Chem. Rev.* **1985**, *85*, 219. (e) König, E. *Struct. Bonding (Berlin)* **1991**, *76*, 51. (f) Lawthers, I.; McGarvey, J. J. *J. Am. Chem. Soc.* **1984**, *106*, 4280. (g) Decurtins, S.; Gütlich, P.; Hasselbach, K. M.; Spiering, H.; Hauser, A. *Inorg. Chem.* **1985**, *24*, 2174. (h) Decurtins, S.; Gütlich, P.; Köhler, C. P.; Spiering, H.; Hauser, A. *Chem. Phys. Lett.* **1984**, *105*, 1.

(3) Sorai, M.; Seki, S. *J. Phys. Chem. Solids* **1974**, *35*, 555.

(4) Slichter, C. P.; Drickamer, H. G. *J. Chem. Phys.* **1972**, *56*, 2142.

10.1021/ic0100976 CCC: $20.00
Published on Web 06/26/2001

the cationic complexes $[Fe(L)_x]^{2+}$ where x is 2, 3, or 6 for tridentate, didentate, or monodentate ligands, respectively. These cationic species condense in the solid state with a large variety of noncoordinating counteranions, which influence dramatically the spin-crossover behavior. The other family includes neutral compounds $[Fe(L)_y(A)_2]$ where $y = 2$ or 4 and L is a didentate or monodentate ligand, respectively, which impart stronger ligand field than in the $[Fe(L)_x]^{2+}$ cationic complexes. The ligand A is almost invariably the anionic ligand NCS^- or $NCSe^-$. Halides or pseudohalides like N_3^- and NCO^- afford HS compounds, while LS compounds can be obtained with strong-field ligands like CN^-.[2b] Hence, the choice of anionic ligands for the synthesis of neutral spin-crossover complexes is still very limited. In this context, the synthesis and characterization of new neutral spin-crossover compounds based on the didentate and monodentate anions 1-*H*-dihydro-bis-pyrazolylborate[6] and the monodentate anion $TCNQ^-$ (tetracyanoquinodimethane),[7] respectively, have been recently reported.

The synthesis of new spin-crossover compounds is of utmost importance for this research area, particularly when the syntheses have to be performed in a controlled manner with the aim of obtaining compounds exhibiting predictable spin-crossover behaviors. Recently, we have reported the synthesis and characterization of the spin-crossover system $[Fe(abpt)_2(NCX)_2]$ where abpt is 4-amino-3,5-bis(pyridin-2-yl)-1,2,4-triazole and X = S, Se.[8] Both compounds are isostructural, showing very similar pseudo-octahedral geometries with the pseudohalide ligands in trans position. Investigation of the spin-crossover conversion was carried out by magnetic, calorimetric, and photomagnetic studies. Following this research we have explored the possibilities of the dicyanamide $[N(CN)_2]^-$, a ligand which can be considered in a first approximation similar to the anionic groups SCN^-, $SeCN^-$, or $TCNQ^-$ as they have in common the $R-CN^-$ donor group. The $[N(CN)_2]^-$ ligand is the object of considerable attention not only because it is a versatile building block for multidimensional frameworks[9] but also because it is an efficient transmitter of magnetic interaction. For instance, in the case of three-dimensional complexes $M[N(CN)_2]_2$ (M = V, Cr, Mn, Fe, Co, Ni, Cu) magnetic ordering has been observed.[9]

As far as we are aware no report on spin-crossover complexes containing the dicyanamide ligand has been reported up to now. Herein we present the synthesis and characterization of $\{Fe(abpt)_2[N(CN)_2]_2\}$, which represents the first example of a spin-crossover complex containing the dicyanamide ligand.

Experimental Section

Materials. 4-Amino-3,5-bis(pyridin-2-yl)-1,2,4-triazole (Aldrich), $FeSO_4 \cdot 7H_2O$ (Panreac), and $NaN(CN)_2$ (Aldrich) were used as received.

Table 1. Crystallographic Data for $\{Fe(abpt)_2[N(CN)_2]_2\}$

empirical formula	$C_{28}H_{20}Fe_1N_{18}$	V, Å^3	710.44(7)
fw	664.47	Z	1
space group	$P\bar{1}$ (2)	T, K	293(2)
a, Å	8.4618(5)	λ, Å	0.71073
b, Å	9.6086(3)	μ, mm^{-1}	0.588
c, Å	9.6381(7)	ρ_{calc}, g/cm^3	1.553
α, deg	83.661(4)	R1[a]	0.0340
β, deg	86.642(5)	wR2[a]	0.0904
γ, deg	65.821(4)		

[a] $R1 = \sum||F_o| - |F_c||/\sum|F_o|$; $wR2 = [\sum[w(F_o^2 - F_c^2)^2/\sum[w(F_o^2)^2]]^{1/2}$. $w = 1/[\sigma^2(F_o^2) + (0.0522P)^2 + 0.1930P]$ where $P = (F_o^2 + 2F_c^2)/3$.

Table 2. Selected Bond Distances (Å) and Angles (deg)[a] for $\{Fe(abpt)_2[N(CN)_2]_2\}$

Fe−N(1)	2.216(2)	C(13)−N(8)	1.300(3)
Fe−N(2)	2.121(2)	N(8)−C(14)	1.307(3)
Fe−N(3)	2.160(2)	C(14)−N(9)	1.137(3)
N(3)−C(13)	1.145(3)		
N(1)−Fe−N(2)	75.17(6)	N(2)−Fe−N(3)	89.10(6)
N(1)−Fe−N(3)	90.28(6)	C(13)−N(8)−C(14)	121.4(2)

[a] Numbers in parentheses are estimated standard deviations in the least significant digit.

Preparation of $\{Fe(abpt)_2[N(CN)_2]_2\}$. To a solution of abpt (0.5 mmol, 119 mg) in methanol (20 mL) was added a water/methanol (1:1) solution (40 mL) of $FeSO_4 \cdot 7H_2O$ (0.25 mmol, 69.5 mg). The resulting orange solution was mixed with a solution of $NaN(CN)_2$ (0.5 mmol, 44.5 mg) in water (20 mL). The final solution was filtered and allowed to evaporate for a week, giving orange crystals of $\{Fe(abpt)_2[N(CN)_2]_2\}$ suitable for X-ray studies. All manipulations were performed in an argon atmosphere. Yield: 50%. Anal. Calcd for $C_{28}H_{20}N_{18}Fe$: C, 50.62; H, 3.03; N, 37.94. Found: C, 50.22; H, 2.96; N, 38.14.

X-ray Crystallography. Diffraction data for $\{Fe(abpt)_2[N(CN)_2]_2\}$ was collected at room temperature with an Enraf-Nonius CAD-4 diffractometer using graphite-monochromated Mo Kα radiation with the $\omega-2\theta$ scan method (see Table 1). The unit-cell parameters were determined from least-squares refinement on the setting angles from 25 centered reflections in the range $12° < \theta < 20°$. No significant fluctuations were observed in the intensities of three standard reflections monitored periodically throughout data collections.

The structure of $\{Fe(abpt)_2[N(CN)_2]_2\}$ was solved by standard Patterson methods and refined by the full-matrix least-squares method on F^2. The computations were performed by using SHELXS86 and SHELXL93.[10] All non-hydrogen atoms were refined anisotropically. The final full-matrix least-squares refinement, minimizing $\sum w[(|F_o|)^2 - (|F_c|)^2]^2$, converged at the values of R1 and wR2 listed in Table 1. The molecular plots were drawn with the ORTEP program.[11] Table 2 gathers selected interatomic bond distances and angles.

Magnetic Susceptibility and Photomagnetic Measurements. The variable-temperature magnetic susceptibility measurements were carried out on microcrystalline samples using a Quantum Design MPMS2 SQUID susceptometer equipped with a 55 kG magnet and operating in the ranges 0.1−1 T and 1.8−300 K. The susceptometer was calibrated with $(NH_4)_2Mn(SO_4)_2 \cdot 12H_2O$. Experimental susceptibilities were corrected for diamagnetism of the constituent atoms by the use of Pascal's constants. Photomagnetic experiments were carried out using a Xe lamp with a 550 nm filter coupled through an optical fiber to the SQUID magnetometer; the output power was 2 mW cm^{-2}.

Results

Crystal Structure. Figure 1 shows a perspective drawing of $\{Fe(abpt)_2[N(CN)_2]_2\}$ together with the atom-numbering scheme. $\{Fe(abpt)_2[N(CN)_2]_2\}$ crystallizes in the triclinic $P\bar{1}$ space group.

(5) (a) Buhks, E.; Navon, G.; Bixon, M.; Jortner, J. *J. Am. Chem. Soc.* **1980**, *102*, 2918. (b) Beattie, J. K. *Adv. Inorg. Chem.* **1988**, *32*, 2. (c) Xie, C. L.; Hendrickson, D. N. *J. Am. Chem. Soc.* **1987**, *109*, 6981. (d) Hauser, A. *Comments Inorg. Chem.* **1995**, *17*, 17. (e) Hauser, A.; Jeftic, J.; Romstedt, H.; Hinek, R.; Spiering, H.; Gütlich, P. *Coord. Chem. Rev.* **1999**, *190−192*, 471.

(6) Real, J. A.; Muñoz, M. C.; Faus, J.; Solans, X. *Inorg. Chem.* **1997**, *36*, 3008.

(7) Kunkeler, P. J.; Koningsbruggen, P. J.; Cornelissen, J. P.; Horst, A. N.; Kraan, A. M.; Spek, A. L.; Haasnoot, J. G.; Reedijk, J. *J. Am. Chem. Soc.* **1996**, *118*, 2190.

(8) Moliner, N.; Muñoz, M. C.; Létard, S.; Létard, J.-F.; Solans, X.; Burriel, R.; Castro, M.; Kahn, O.; Real, J. A. *Inorg. Chim. Acta* **1999**, *291*, 279.

(9) (a) Jensen, P.; Price, D. J.; Batten, S. R.; Moubaraki, B.; Murray, K. S. *Chem.−Eur. J.* **2000**, *6*, 3186 and references therein. (b) Batten, S. R.; Harris, A. R.; Jensen, P.; Murray, K. S.; Ziebell, A. *J. Chem. Soc., Dalton Trans.* **2000**, 3829 and references therein.

(10) Sheldrick, G. M. SHELXS86. *Acta Crystallogr.* **1990**, *A46*, 467; *SHELXL93, Program for the Refinement of Crystal Structures*; University of Göttingen: Göttingen, 1993.

(11) Johnson, C. K. ORTEP. Report ORNL-3794; Oak Ridge National Laboratory: Oak Ridge, TN, 1971.

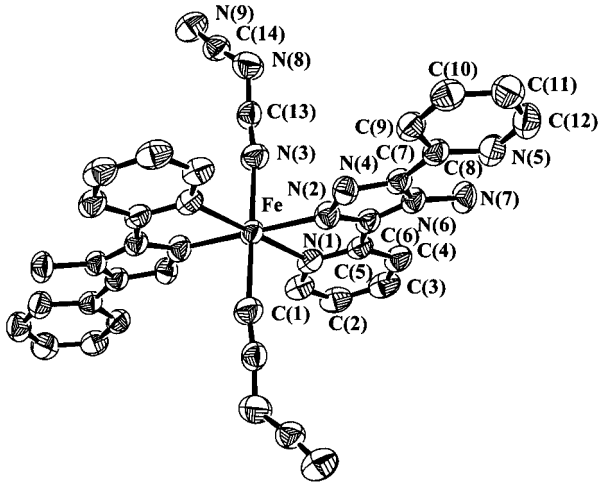

Figure 1. Perspective view of the $\{Fe(abpt)_2[N(CN)_2]_2\}$ molecule at 293 K, including the non-hydrogen atom numbering. Hydrogen atoms are omitted for clarity.

The unit cell contains a centrosymmetric mononuclear $\{Fe(abpt)_2[N(CN)_2]_2\}$ species. Each iron atom is in a distorted octahedral $[FeN_6]$ environment. The four basal nitrogen atoms coordinated to the iron atom belong to the pyridyl [N(1)] and triazole [N(2)] groups of two equivalent abpt ligands. The remaining trans positions are occupied by two nitrogen atoms [N(3)] belonging to two $[N(CN)_2]^-$ anions. The Fe−N bond distances involving the pyridyl groups [Fe−N(1) = 2.216 (**2**) Å] are larger than those corresponding to the triazole rings [Fe−N(2) = 2.121(2) Å] and the $[N(CN)_2]^-$ groups [Fe−N(3) = 2.160(2) Å]. The bite angle N(1)−Fe−N(2) = 75.17(6)° strongly differs from 90° as expected for this kind of α-diimine ligands. The remaining cis nitrogen atoms are found in the range 89−91°. The $[N(CN)_2]^-$ group is angular, and the C(13)−N(8)−C(14) angle is equal to 121.4(2)°, with the two N−C−N moieties nearly linear (171.1(2)° and 170.9(2)°).The nitrogen atoms, N(5) and N(7), of the uncoordinated pyridyl and amino groups, respectively, define an intramolecular hydrogen bond [N(5)···N(7) = 2.896(3) Å, N(7)−H(7B) = 0.94(3) Å, N(5)···(7) = 2.848(12) Å, N(5)···H(7B)···N(7) = 139(2)°]. Consequently, an almost planar configuration is observed for the abpt ligand. The dihedral angle defined by the uncoordinated pyridyl and the triazole moieties is 8.31(13)°. This fact has been previously reported for other mononuclear abpt compounds.[7,8,12] The crystal packing of $\{Fe(abpt)_2[N(CN)_2]_2\}$, seen in the [100] direction ($y-z$ plane), consists of linear chains made of $\{Fe(abpt)_2[N(CN)_2]_2\}$ units, which stack parallel to the [001] direction (see Supporting Information). Inside each chain, cohesion stems from $\pi-\pi$ interactions between the complex units related by a crystallographic inversion center, located at the iron atom. The average distance between overlapping ligands is ca. 3.6 Å. The number and intensity of intermolecular contacts decrease dramatically along the [100] and [001] directions. However, it is worth noting that relatively strong intermolecular contacts (3.2 Å) occur between C(1)−C(2′) and C(2)−C(1′) which define two-dimensional networks spreading in the $x-z$ plane.

Magnetic Properties. Figure 2 shows the thermal dependence of the $\chi_M T$ product for $\{Fe(abpt)_2[N(CN)_2]_2\}$ (open circles), χ_M being the molar magnetic susceptibility and T the temperature. At room temperature, $\chi_M T$ is equal to 3.32 cm^3 K mol^{-1}, which is in the range of values expected for an iron(II) ion in the HS state. As the temperature is lowered, $\chi_M T$ first remains constant and then decreases abruptly from 150 K down to 60 K. Interestingly, in the middle of the transformation ($\chi_M T \approx 1.6-1.8$ cm^3 K mol^{-1}) the slope of the $\chi_M T$ vs T curve diminishes significantly. The plateau observed in the region of temperature 60−25 K corresponds to 1.23 cm^3 K mol^{-1}. These features reveals an incomplete HS ↔ LS spin conversion occurring in two steps. The incomplete second step involves around 37% of HS molecules trapped at low temperatures. The subsequent dropping of $\chi_M T$ at temperatures below 25 K corresponds most probably to the occurrence of zero-field splitting of the remainder of HS iron(II) ions. Despite the singular character of the spin transition, we have made a rough estimate of the thermodynamic parameters, which account for the main features of the spin conversion in $\{Fe(abpt)_2[N(CN)_2]_2\}$, using the Slichter and Drickamer model derived from the regular solution theory:[4]

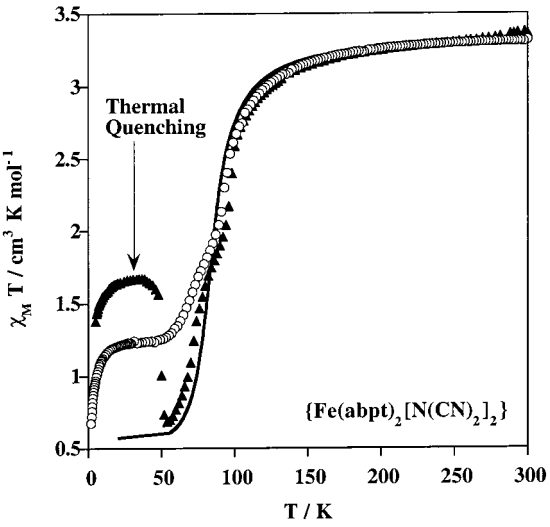

Figure 2. $\chi_M T$ versus T plots for $\{Fe(abpt)_2[N(CN)_2]_2\}$. Sample was cooled from 300 to 2 K at 2 K min^{-1} (open circles). Thermal quenching: sample was cooled from 300 to 5 K at 100 K min^{-1} and then warmed slowly (black triangles, see text). The solid line corresponds to simulation of the experimental spin conversion (see text).

$$\ln[(1-n_{HS})/(n_{HS}-f_{HS})] = [\Delta H + \Gamma(f_{HS}+1-2n_{HS})]/RT - \Delta S/R \quad (1)$$

$$n_{HS} = \frac{(\chi_M T)_m}{(\chi_M T)_{HS}} \quad (2)$$

where n_{HS} represents the HS molar fraction, $(\chi_M T)_{HS}$ and $(\chi_M T)_m$ represent the $\chi_M T$ value at 100% of conversion (3.32 cm^3 K mol^{-1}) and at different temperatures, respectively, f_{HS} is the HS molar fraction trapped at low temperatures, 17% for the most complete conversion (filled triangles in Figure 2, see below). The variation of enthalpy, ΔH, and entropy, ΔS, and the intermolecular interaction term Γ obtained from simulation of the experimental data (see solid line in Figure 2) are 3.5 kJ mol^{-1}, 41 J K^{-1} mol^{-1}, and 0.9 kJ mol^{-1}, respectively. The thermodynamic parameters estimated for the title compound are quite reasonable for a spin transition which takes place at $T_{1/2}$ = 86 K ($T_{1/2} = \Delta H/\Delta S$ is the characteristic temperature at which 50% of conversion takes place). $T_{1/2}$ = 86 K is one of the lowest temperatures observed for an iron(II) spin-crossover com-

(12) (a) Cornelissen, J. P.; Diemen, J. H.; Groeneveld, L. R.; Haasnoot, J. G.; Spek, A. L.; Reedijk, J. *Inorg. Chem.* **1992**, *31*, 198. (b) Faulmann, C.; Koningsbruggen, P. J.; Graaff, R. A. G.; Haasnoot, J. G.; Reedijk, J. *Acta Crystallogr.* **1990**, *C46*, 2357. (c) García, M. P.; Manero, J. A.; Oro, L. A.; Apreda, M. C.; Cano, F. H.; Foces-Foces, C.; Haasnoot, J. G.; Prins, R.; Reedijk, J. *Inorg. Chim. Acta* **1986**, *122*, 235.

pound. Observation of important amounts of trapped HS molecules at low temperature is usually ascribed to the occurrence of two different sites in the crystal.[13] One of the sites imparts weaker ligand field strength and, consequently, stabilizes HS molecules whereas the other with a stronger ligand field stabilizes spin-crossover centers. Texture effects or occurrence of different polymorphs, one of them being paramagnetic in the whole range of temperatures, has been also claimed.[2b−d]

Due to the low temperatures involved in the spin transition of the title compound, it is reasonable to take into consideration that slow kinetics could block the LS ↔ HS equilibrium.

Dynamics of the Spin Conversion. Thermal Quenching. We have performed thermal quenching experiments by cooling the sample rapidly (≈100 K min^{-1}) from room temperature down to 5 K to demonstrate that slow kinetics effects are present in the system. Figure 2 displays the magnetic behavior of the quenched sample at increasing temperatures (filled triangles). At 5 K, $\chi_M T$ is equal to 1.40 cm^3 K mol^{-1}. This value represents apparently 43% of trapped HS molecules. A progressive increase of $\chi_M T$ was observed as the sample was slowly warmed (2 K min^{-1}). The thermal dependence of $\chi_M T$ attains a maximum value of 1.70 cm^3 K mol^{-1} in the range of temperatures 25−38 K. The increase of $\chi_M T$ corresponds, most probably, to the occurrence of zero-field splitting in the $S = 2$ ground state of the trapped HS molecules. Hence, the effective thermal quenching at low temperature actually involves around 50% of molecules in the HS state. In the range of temperatures 45−62 K, $\chi_M T$ diminishes as a consequence of HS → LS relaxation. In this range of temperatures, $\chi_M T$ was registered every 2 K after a long wait for each temperature in order to reach the thermodynamic equilibrium. The sequence, with delays given in parentheses, was the following: 48 K (60 min), 50 K (120 min), 52 K (120 min), 54 K (60 min), 56 K (60 min), 58 K (30 min), 60 K (30 min), and 62 K (15 min). As can be seen in Figure 2, $\chi_M T$ falls up to ca. 0.69 cm^3 K mol^{-1} at 52 K. Obviously, greater delays would produce smaller $\chi_M T$ values according to a greater extent of the HS → LS relaxation.

For temperatures higher than 52 K, the molecules absorb sufficient energy to overcome the energy barrier between the two LS and HS potential wells. Consequently, both, normal regime and thermal quenching experiments superpose above $T = 68$ K.

Relaxation Studies of the Quenched HS State to the LS State. The dynamics of the HS → LS relaxation has been investigated in the temperature range 10−60 K. The decays of the quenched HS molar fraction normalized to 1 at time zero, n_{HS}, versus time at various temperatures are presented in Figure 3. In the range of temperatures 10−25 K the relaxation is very small. The rate constant $k_{HL}(T)$ has been obtained from the simple exponential behavior

$$n_{HS} = \exp(-k_{HL}(T)t) \qquad (3)$$

For temperatures in the range 30−60 K the decay shows a strong deviation from single exponential. The n_{HS} vs t curves follow a stretched exponential law. Stretched exponential decay depends on the relative amounts of HS and LS species in the sample and corresponds to fast initial decays followed by a progressively much slower decay. It has been proposed to

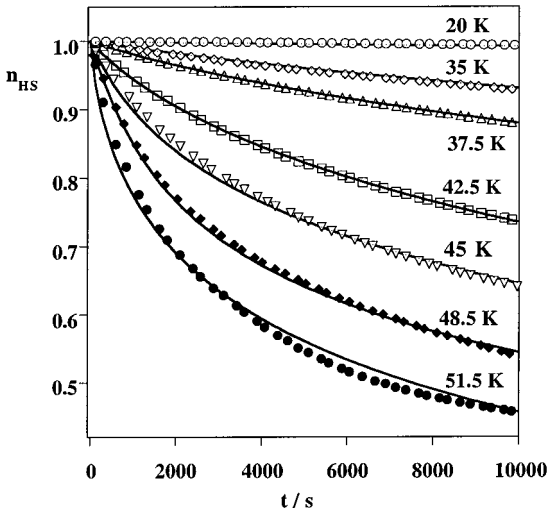

Figure 3. Time dependence at various temperatures of the normalized HS molar fraction, n_{HS}, generated by thermal quenching. Solid lines represent the best fit to the experimental HS → LS relaxation curves at different temperatures.

analyze n_{HS} vs t curves as a distribution of relaxation rates k_{HL}, related to a repartition of activation energies. At a given temperature, k_{HL} can be obtained by using a Gaussian distribution of energies centered at E_0 with standard deviations and a pre-exponential factor k_0.[14] The Arrhenius plot, ln[$k_{HL}(T)$] vs $1/T$, for {Fe(abpt)$_2$[N(CN)$_2$]$_2$} according to

$$k_{HL}(T) = A_{HL} \exp(-E_a/k_b T) \qquad (4)$$

where A_{HL} is the preexponential factor and E_a corresponds to the thermal activation energy of the process, displays two characteristic regions, one where the process is thermally activated ($E_a \approx 280$ cm^{-1}, $A_{HL} \approx 10$ s^{-1}) and an almost temperature independent region corresponding to the tunneling relaxation ($k_0^{HL}(10\text{ K}) \approx 1.2 \times 10^{-4}$ s^{-1}) (see Supporting Information).

Photomagnetic Measurements. **LIESST Experiment.** The LIESST experiment was carried out on a microcrystalline sample of {Fe(abpt)$_2$[N(CN)$_2$]$_2$}. Figure 4 shows the results. The magnetic response was measured first in the cooling mode (1 K min^{-1}) from 200 K down to 5 K with an applied magnetic field of 2 T (black rhombuses). At 5 K, the sample was irradiated for 90 min, the time required to attain the saturation value of $\chi_M T = 1.8$ cm^3 K mol^{-1} (open triangles). The light irradiation was then turned off, and the temperature was increased at the rate of 0.3 K min^{-1} in the temperature region 5−150 K (open circles). $\chi_M T$ increased progressively up to 2.9 cm^3 K mol^{-1} at 38 K. Taking into account the occurrence of ZFS in the low-temperature region, an almost quantitative LIESST effect has been achieved for {Fe(abpt)$_2$[N(CN)$_2$]$_2$}. At temperatures greater than 38 K, $\chi_M T$ drops rapidly to reach the minimum value, 1.3 cm^3 K mol^{-1}, at 55 K indicating the occurrence of HS → LS relaxation. At temperatures greater than 55 K, $\chi_M T$ increases again following the two-step transition observed in the cooling mode. The characteristic critical temperatures corresponding to the maximum variation of $\chi_M T$ in the HS → LS relaxation after LIESST, $T_{cliesst}$,[15] and to the first, T_{c1}, and second steps, T_{c2}, of the spin transition are 52, 72, and 96 K, respectively.

Study of the HS → LS Relaxation after the LIESST Effect. The dynamics of the HS → LS relaxation after the LIESST

(13) (a) Poganiuch, P.; Decurtins, S.; Gütlich, P. *J. Am. Chem. Soc.* **1990**, *112*, 3270. (b) Poganiuch, P.; Gütlich, P. *Hyperfine Interact.* **1988**, *40*, 331. (c) Buchen, T.; Poganiuch, P.; Gütlich, P. *J. Chem. Soc., Dalton Trans.* **1994**, 2285. (d) Hinek, R.; Spiering, H.; Schollmeyer, D.; Gütlich, P.; Hauser, A. *Chem.—Eur. J.* **1996**, *2*, 1127.

(14) Hauser, A.; Adler, J.; Gütlich, P. *Chem. Phys. Lett.* **1988**, *152*, 468.

(15) Létard, J. F.; Capes, L.; Chastanet, G.; Moliner, N.; Létard, S.; Real, J. A.; Kahn, O. *Chem. Phys. Lett.* **1999**, *313*, 115.

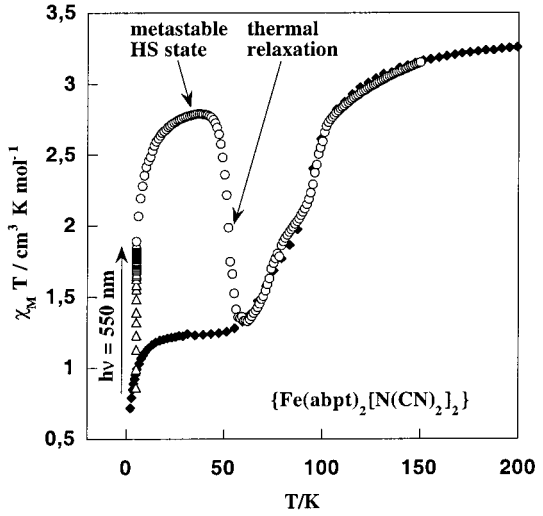

Figure 4. $\chi_M T$ versus T plots for $\{Fe(abpt)_2[N(CN)_2]_2\}$. Sample was cooled from 300 to 5 K at 2 K min^{-1} (black rhombuses), then irradiated (550 nm) for 90 min at 5 K (open triangles), and finally warmed (0.3 K min^{-1}) after light irradiation was turned off.

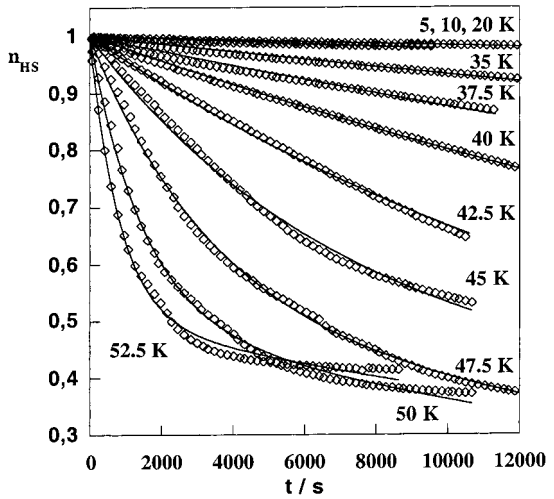

Figure 5. Time dependence at various temperatures of the normalized HS molar fraction, n_{HS}, generated by the LIESST effect. Solid lines represent the best fit to the experimental HS → LS relaxation curves at different temperatures.

effect was investigated from 5 K up to 52.5 K. For higher temperatures, relaxation was too fast relative to the SQUID time window. Additionally, at these temperatures thermal population of the HS state becomes an important process due to the low temperature T_{c1}. The decay of the normalized HS molar fraction, n_{HS}, versus time at various temperatures is presented in Figure 5. A single-exponential law was used for fitting relaxation in the range of temperatures 5−45 K. For higher temperatures the fitting procedure was similar to that described in the relaxation studies of the quenched HS state. The Arrhenius plot $\ln[k_{HL}(T)]$ vs $1/T$ shows again the above-mentioned regions, one characterized by a k_{HL} very small and temperature independent where the tunneling mechanism is predominant (k^o_{HL} (5 K) ≈ 1.74×10^{-6} s^{-1}) and the other where k_{HL} is mostly thermally activated ($E_a \approx 431$ cm^{-1}, $A_{HL} \approx 144$ s^{-1}) (see Supporting Information).

Discussion

$\{Fe(abpt)_2[N(CN)_2]_2\}$ has a molecular structure very similar to that previously reported for $[Fe(abpt)_2(NCX)_2]$ (X = S, Se).[8]

Table 3. Significant Structural Data of the $\{Fe(abpt)_2(X)_2\}$ Family (X = $NCSe^-$, NCS^-, and $[N(CN)_2]^-$)

	X = $NCSe^-$	X = NCS^-	X = $[N(CN)_2]^-$
Fe−N(pyridine) (Å)	2.189(8)	2.205(5)	2.217(5)
Fe−N(triazole) (Å)	2.105(8)	2.120(4)	2.121(2)
Fe−N(X) (Å)	2.131(9)	2.120(5)	2.160(2)
$R[FeN_6]$ (Å)	2.142(9)	2.148(5)	2.166(5)
dihedral angle (deg)	8.0	8.5	8.3

The average Fe−N bond distances, $R[FeN_6]$, are 0.024 and 0.018 Å shorter in the NCS^- and $NCSe^-$ derivatives, respectively, and constitute the main structural difference with respect $\{Fe(abpt)_2[N(CN)_2]_2\}$ (see Table 3). Intermolecular hydrogen bonding between the amine group of the triazole ring and the nitrogen atom of the uncoordinated pyridine ring takes place in the three compounds. This fact is the reason why the three derivatives show similar small dihedral angles between the triazole and the uncoordinated pyridine rings in such a way that the abpt ligands remain almost planar. The abpt ligands of two adjacent complex molecules interact via $\pi-\pi$ stacking describing infinite chains of molecules $[Fe(abpt)_2(NCX)_2]$ (X = S, Se, NCN). Despite this similitude among the three compounds, the S and Se derivatives, which are isostructural, crystallize in the monoclinic system (space group $P2_1/n$) while $\{Fe(abpt)_2[N(CN)_2]_2\}$ crystallizes in the triclinic system (space group $P\bar{1}$). However, the most important difference corresponds to the number and intensity of the intermolecular contacts between adjacent molecules belonging to different parallel chains. Whereas the intermolecular contacts are weak in the NCS^- and $NCSe^-$ derivatives, they are stronger for the $N(CN)_2^-$ derivative, the shorter C1−C2′ and C2−C1′ intermolecular distances being around 3.2 Å.

Concerning the nature of the spin conversion, $\{Fe(abpt)_2[N(CN)_2]_2\}$ shows two remarkable singularities. On one hand, it exhibits one of the lowest $T_{1/2}$ values observed in an iron(II) spin-crossover compound (86 K). This fact has allowed us to observe and analyze the kinetic effects responsible for the incomplete character of the spin transition. The trapping experiments have shown that, in the warming mode of the sample at rates as slow as 0.028 K min^{-1}, the metastable HS state relaxes back to the LS ground state. The relaxation takes place with greater efficiency than in the standard warming procedure (1−2 K min^{-1}) where 37% of molecules remain in the HS state at low temperature. For temperatures greater than 65 K the population of the HS state becomes more favorable and $\chi_M T$ increases. On the other hand, the occurrence of two-step conversion deserves to be mentioned. Two-step spin conversions have been previously observed in mononuclear and polynuclear compounds. The first compound for which a two-step spin conversion was observed is $[Fe(2\text{-pic})_3]Cl_2 \cdot EtOH$, (2-pic = 2-picolylamine).[16] In this compound, there is a unique iron crystallographic site, and consequently the two-step conversion has been attributed to a competition between long-range cooperative and short-range anticooperative interactions.[17,18] A similar explanation has been drawn for the two-step transition observed in $[Fe(5\text{-}NO_2\text{-sal-N}(1,4,7,10)]$, where 5-$NO_2$-sal-N(1,4,7,10) is a hexadentate ligand arising from the Schiff base condensation of 5-NO_2-salicylaldehyde with 1,4,7,10-tetraazadecane. In this compound, the two-step conversion was

(16) Köppen, H.; Müller, E. N.; Khöler, C. P.; Spiering, H.; Meissner, E.; Gütlich, P. *Chem. Phys. Lett.* **1982**, *91*, 348.
(17) Jakobi, R.; Spiering, H.; Gütlich, P. *J. Phys. Chem. Solids* **1992**, *53*, 267.
(18) Köhler, C. P.; Jakobi, R.; Meissner, E.; Wiehl, L.; Spiering, H.; Gütlich, P. *J. Phys. Chem. Solids* **1990**, *51*, 239.

associated with structural phase transitions evidenced by X-ray diffraction studies at various temperatures.[19] The crystal structure of {Fe(abpt)$_2$[N(CN)$_2$]$_2$} only shows, as in [Fe(2-pic)$_3$]Cl$_2$·EtOH, the occurrence of one type of crystallographic iron atom at room temperature. We have no evidence of a structural crystallographic transition at low temperatures for the title compound.

The characteristic transition temperatures $T_{1/2}(NCSe^-) = 224$ K, $T_{1/2}(NCS^-) = 180$ K, and $T_{1/2}(N(CN)_2^-) = 86$ K seem to be related to the electronegativity of the pseudohalide. The estimated Sanderson's electronegativities are 2.84, 2.66, and 2.60 for $[N(CN)_2]^-$, NCS^-, and $NCSe^-$, respectively,[20] the more electronegative the lower $T_{1/2}$ is observed for the [Fe(abpt)$_2$(NCX)$_2$] series.The LIESST experiments have allowed us to study the dynamics of the HS → LS relaxation process. Thermal activation and tunneling are the two predominant mechanisms accounting for the relaxation rate at temperatures greater and smaller than 35 K, respectively. In the theory of nonadiabatic multiphonon relaxation[5a] the low-temperature tunneling rate can be expressed as

$$k_{HL}^{o} = \frac{2\pi}{\hbar\omega} H_{HL}^{2} g_L \frac{S^p \exp(-S)}{p!} \qquad (5)$$

where H_{HL} is the electronic matrix element $\langle\psi_{HS}|H_{SO}|\psi_{LS}\rangle$, which is estimated to be around 150 cm^{-1},[5d] and $g_L = 1$ is the electronic degeneracy of the final state LS. S represents the Huang−Rhys factor, which is a measure of the horizontal displacement of the HS and LS wells,

$$S = \frac{1}{2} f \frac{\Delta Q_{HL}^{2}}{\hbar\omega} \qquad (6)$$

where f, ΔQ_{HL}, and $\hbar\omega$ are the Fe−N bond force constant, the reduced coordinate change ($\Delta Q_{HL} = \sqrt{6}\Delta R_{HL}$), and the characteristic frequency of the [FeN$_6$] core, respectively. The parameter p is the reduced energy gap, $\Delta E_{HL}^{o}/\hbar\omega$, between the two wells. It seems reasonable to consider, in a first approximation, that ΔH obtained from the calorimetric measurements or estimated from the thermal variation of n_{HS} is close to the corresponding ΔE_{HL}^{o}. An estimation of the characteristic $\hbar\omega = 260$ cm^{-1} has been obtained from the Raman spectra of [Fe(abpt)$_2$(NCS)$_2$] registered at 100 K where the compound is in the LS state.[21] Considering that the $\hbar\omega$ value should not change significantly for $NCSe^-$ and $N(CN)_2^-$ derivatives, p can be estimated for the three derivatives (see Table 4). Consequently, the corresponding S values can be graphically deduced from expression 5 when the rate constant estimated at the lowest temperature is considered as k_{HL}° (see Supporting Information). The S values estimated in this way enable us, through expression 6, to obtain the value $\Delta R_{HL} \approx 0.18-0.19$ Å, which is consistent with $f \approx 2.2 \times 10^5$ dyn cm^{-1}. Both ΔR_{HL} and f values have been roughly evaluated but, however, are in good agreement with what is expected for iron(II) spin-crossover complexes.[2e,5d]

Table 4. Relevant Thermodynamic and Kinetic Data of the {Fe(abpt)$_2$(X)$_2$} Family (X = $NCSe^-$, NCS^-, and $[N(CN)_2]^-$)

	$T_{1/2}$/K	ΔH/cm^{-1}	k_{HL}°/s^{-1}	p	S
$[N(CN)_2]^-$	84	291	1.7×10^{-6}	1.12	45
NCS^-	184	482	1.3×10^{-4}	1.85	43
$NCSe^-$	220	715	7.6×10^{-4}	2.75	44

It should be mentioned that the two relaxation processes here described show different HS → LS relaxation rates. In the high-temperature range, where the process can be considered mainly thermally activated, relaxation is faster in the quenching experiment than in relaxation after the LIESST effect. In the former case, a maximum of 50% of HS molecules are randomly "created" in a LS matrix. Hence, because of the difference in size between LS and HS molecules, an internal pressure is built up against the HS molecules, which consequently accelerates the HS → LS decay. In this regime, correlation and random distribution of molecules in the HS state cause a distribution of energy separations by the short-range interactions,[22] and in turn a distribution of decay times. The k_{HL} for a random distribution of HS state molecules is an average rate constant. In contrast to this, the HS → LS relaxation after the LIESST effect where almost 100% of molecules are in the HS state is characterized by smaller decay times.

Finally, in the predominant tunneling region the estimated k_{HL} constants for the quenching experiments are noticeably greater (2 orders of magnitude) than those of relaxation after the LIESST process. It may be explained from the cooperative effects on the zero-point gap energy ΔE_{HL}^{o}. In the mean field approximation ΔE_{HL}^{o} increases linearly as a function of the LS fraction. This results in a self-acceleration rate constant for the HS → LS relaxation.[22]

Acknowledgment. We are grateful for financial support from the European Commision for granting the TMR_Network "Thermal and Optical Switching of Spin States (TOSS)", Contract No. ERB-FMRX-CT98-0199EEC/TMR. We thank the Spanish DGICYT for financial assistance through Project PB97-1397.

Supporting Information Available: Tables of X-ray crystallographic data for {Fe(abpt)$_2$[N(CN)$_2$]$_2$}, structural projection along the [100] direction, Arrhenius plots for the quenching and LIESST relaxation experiments, and graphical evaluation of S. This material is available free of charge via the Internet at http://pubs.acs.org.

IC0100976

(19) Boinnard, D.; Bousseskou, A.; Dworkin, A.; Savariault, J. M.; Varret, F.; Tuchagues, J. P. *Inorg. Chem.* **1994**, *33*, 271.
(20) Sanderson, R. T. *Simple Inorganic Substances*; Robert E. Krieger Pub. Co.: Melbourne, FL, 1989.
(21) Moliner, N. Ph.D. Thesis, Universitat de València, 2000.
(22) Spiering, H.; Kohlhaas, T.; Romstedt, H.; Hauser, A.; Bruns-Yilmaz, C.; Kusz, J.; Gütlich, P. *Coord. Chem. Rev.* **1999**, *190−192*, 629.